Motions of Short DNA Duplexes: An Analysis of DNA Dynamics Using an EPR-Active Probe†

Eric J. Hustedt,‡ Andreas Spaltenstein, James J. Kirchner, Paul B. Hopkins, and Bruce H. Robinson*

Department of Chemistry, University of Washington, Seattle, Washington 98195

Received July 20, 1992; Revised Manuscript Received November 18, 1992

ABSTRACT: The dynamics of a series of four DNA duplexes of length 12, 24, 48, and 96 base pairs have been studied using an electron paramagnetic resonance (EPR) active nitroxide spin-label covalently attached to a thymidine located near the center of each duplex. The linear EPR spectra were simulated by solving the stochastic Liouville equation for anisotropic rotational diffusion. The diffusion tensor for global rotation of the duplex was predicted from hydrodynamic theory for a right circular cylinder. All internal motions, assumed to be rapid, are modeled by reduced electron Zeeman and hyperfine tensor anisotropies. Best fit simulations to the data were then obtained by adjusting the total amplitude of all internal dynamics. The local, length-independent and the collective, length-dependent contributions to the internal dynamics were separated by determining the total amplitude of internal motion as a function of duplex length. The major axis of the spin tensors was determined to be tilted 20° from the helix axis. As a result, the spin-label is most sensitive to flexural motions of the DNA duplex. It is found that the global tumbling of the duplex is accurately modeled by hydrodynamic theory. The length-independent motion is characterized by a root-mean-squared amplitude of oscillation of 10° in two dimensions at 20 °C and has a strong temperature dependence, indicating that the local structure of the DNA changes with temperature. The length dependence of the internal dynamics leads to an estimate of the dynamic flexural persistence length of 2500 ± 340 Å. There was no statistically significant difference between models assuming a harmonic or a square-well local bending potential.

Duplex DNA in solution is a semiflexible macromolecule and as such exhibits a complex set of length-dependent dynamic modes. Over the last decade there has been considerable discussion about the dynamic or elastic properties of DNA. The time scales and amplitudes of the internal dynamic processes in duplex DNA are still not fully resolved. Various nuclear magnetic resonance (NMR) experiments have been interpreted in terms of large-amplitude internal motions (20° or greater) (Levy et al., 1983; Kearns, 1984; Eimer et al., 1990). However, Schurr and co-workers have argued that when collective motions are considered, this amplitude reduces to 12° or less (Allison et al., 1982; Schurr & Fujimoto, 1988). Solid-state deuterium NMR studies of hydrated DNA fibers have demonstrated that there are no large-amplitude, high-frequency local base motions (Brandes et al., 1986; Kintanar et al., 1988, 1989). The rather extensive use of different models for internal dynamics has led to large differences in the interpretation of the available data.

In addition, little is known of either the sequence-dependent dynamic properties of DNA or the importance of these properties for long-range DNA structure or protein recognition (Hogan & Austin, 1987; Schultz et al., 1991). Hogan and Austin (1987), citing the example of phage 434 repressor–operator binding which can be dramatically influenced by altering the sequence of the DNA in a region not in direct protein contact, recently suggested that torsional motions may be highly sequence specific. On the other hand, Fujimoto and Schurr (1990) concluded that the sequence-dependent variation in torsional rigidity is insufficient to explain the variation in binding and allowed that the sequence dependence of either the equilibrium structure or the bending rigidity remains as possible explanations for the sequence-specific binding.

Sequence-specific dynamics, with the attendant issues of torsional versus flexural motions and local versus collective internal motions, can be studied at the base pair level using a single local probe placed within the sequence of interest. This approach to exploring the dynamics of DNA provides an alternative to many of the NMR studies and to other techniques, such as time-resolved fluorescence polarization anisotropy (FPA) (Schurr et al., 1992) and transient photodichroism (TPD) (Hogan et al., 1982, 1983), in which the probe is uniformly present throughout the entire DNA duplex. In these latter studies, the results obtained are averages over the entire duplex, including the relatively more flexible base pairs at either end (Allison & Schurr, 1979).

In the following study a nitroxide spin-label is used to monitor the dynamics at a single base pair. Linear continuous-wave electron paramagnetic resonance (CW-EPR) spectra of nitroxide spin-labels are extremely sensitive to dynamic processes whose correlation times are less than 500 ns (Freed, 1976; Robinson et al., 1985; Beth & Robinson, 1989). Motions characterized by correlation times between 1 and 500 ns cause significant changes in line-shape features. Motional processes whose correlation times are less than 1 ns are considered to be in the fast motion limit and have the effect of averaging orientation-dependent EPR resonances into single lines. The motions of short (fewer than 100 base pairs) DNA duplexes can be reasonably categorized according to this same time scale. While the characteristic times for the overall tumbling of the duplex vary depending on length, temperature, and solution viscosity between several to several hundred nanoseconds, the relaxation times for the internal modes generally

† This work was supported in part by grants for the National Science Foundation (DMB-87-06175), the National Institutes of Health (GM 32681), and the Searle Scholars Program. P.B.H. is an NIH Research Career and Development Award recipient (AG 00417).

* Author to whom correspondence should be addressed.

‡ Present address: Department of Molecular Physiology and Biophysics, Vanderbilt University, Nashville, TN 37232.

0006-2960/93/0432-1774$04.00/0

fall below 1 ns. We have taken advantage of this separation of motional effects and consider the overall tumbling explicitly in the simulations of the CW-EPR line shapes, while the more rapid internal motions are treated by considering the averaging effect they have on the EPR resonances. The use of motionally averaged electron Zeeman (g) and hyperfine (A) tensors to account for rapid dynamics was originally developed by McConnell and co-workers and widely applied to the study of lipid dynamics (McConnell & McFarland, 1970; Hubbell & McConnell, 1971; McConnell, 1976; Griffith & Jost, 1976) and recently to hemoglobin-bound spin-labels (Steinhoff et al., 1989). We develop, following Griffith and Jost (1976), a method of obtaining motionally averaged tensors to account for the internal dynamics of spin-labeled DNA. Best fit simulations were then obtained by adjusting a single parameter which is equal to the total mean-squared amplitude of all internal dynamics. This approach is analogous to the model-free approach proposed by Lipari and Szabo (1982a,b) for the interpretation of NMR data. However, our method does not produce any estimate of the correlation times for the internal dynamics.

The site-specific probe used in this work, referred to as T*, is a nitroxide radical attached to an analogue of thymidine via an acetylinic tether (Spaltenstein et al., 1988, 1989a,b). The nature of the tether ensures that there is only one degree of motional freedom of the probe relative to the base and thus minimizes independent probe motion. Bobst and co-workers (Bobst et al., 1984, 1988; Kao & Bobst, 1985; Pauly et al., 1987; Strobel et al., 1990) have developed an alternative set of spin-labels for studying DNA dynamics with longer, less rigid tethers. They analyze their data in terms of anisotropic rotational diffusion with one correlation time dependent on tether length and ascribed to independent probe motion, while the second correlation time is independent of tether and helix length (Bobst et al., 1984) and attributed to motion of the base. The rapid, large-amplitude motions (both of the base and the probe independent of the base) claimed by Bobst and co-workers have not been observed in studies using the T* probe (Spaltenstein et al., 1989a). However, Kirchner et al. (1990) have shown that an analogue of T* with a longer, diacetylinic tether gives an EPR spectrum which shows considerable local motion of the nitroxide due to rotation about the diyne axis. In the case of the monoyne tether of T*, the nitroxide appears to have sufficient steric interaction within the major groove to restrict its local motion but is not in such close contact with the DNA as to disrupt the structure of the duplex. It has been noted as arguments against such structural disruptions that the melting of the self-complementary dodecamer sequence 5′-d(CGCGAATT*CGCG) was quite similar to that of the unlabeled dodecamer and that circular dichroism spectra showed helicity for the spin-labeled as well as the unlabeled dodecamer (Spaltenstein et al., 1988). The presence of small, if any, local influences on dynamics due to the presence of the spin-label should result in an increase in local motion and would have very little effect on the length-dependent, collective internal motions or on the overall tumbling of the DNA duplex.

In this paper we restrict our attention to the four sequences given in Table I. The outer portions of the longer sequences were chosen only to ensure that the sequences were not self-complementary, and by no other criteria. The intent is to keep the spin-label within the same local sequence and always near the center of the molecule. While the intent of this study is to minimize any sequence-dependent dynamic effects, additional studies are being performed to examine this issue. For example, we note that the self-complementary sequence 5′-d(CGCGAATT*CGCG) shows both increased dynamics in the duplex form relative to the 12 base pair sequence in Table I and a duplex–hairpin equilibrium observable by EPR (Hustedt, 1989).

Table I: The Four Spin-Labeled DNA Sequences Studied

N	sequence
12	5′-d(GATAATT*CGTGC)
24	5′-d(GGCGCG-[12-mer]-CGGCGT)
48	5′-d(CCCGATCAGTCT-[24-mer]-ATCCTGCCAACG)
96	5′-d(GCCCGGTAACTGGTGCTAACGCTA-[48-mer]-CTTCGAGTCGGACATTGCCATGTC)

EXPERIMENTAL PROCEDURES

The spin-labeled thymidine, T*, was prepared as described by Spaltenstein et al. (1989b) using both the naturally abundant [^{14}N,H$_{13}$]- and isotopically substituted [^{15}N,D$_{13}$]-nitroxides. Oligomers were prepared on an Applied Biosystems 6800 DNA synthesizer. After synthesis, all oligomers were sized on denaturing polyacrylamide electrophoretic gels (PAGE) and purified on a Sephadex column. The spin-labeled sequences in Table I were then combined with an approximately 20–50% excess of the corresponding unlabeled complementary strands to give between 100 and 300 μM duplex DNA. The buffer in all cases was 0.01 M phosphate adjusted to pH 7, 0.1 mM EDTA, and 0.1 M NaCl. The samples were placed in 50-μL sample tubes. No effort was made to degas the samples. The EPR were recorded digitally on an EPR spectrometer as previously described (Mailer et al., 1985). The samples of DNA were studied at temperatures ranging from 0 to 40 °C. In some experiments, the viscosity was increased by the addition of sucrose.

THEORY

The Stochastic Liouville Equation. The spin response for a particular motional process is given by the quantum mechanical stochastic Liouville equation for the reduced density matrix, $\chi = \sigma - \sigma_{eq}$, which includes the phenomenological spin-relaxation operator, Γ_R, and the stochastic motional operator, Γ_Ω, which describes the random reorientation of the probe relative to the laboratory frame (Freed, 1976; Dalton et al., 1976; Robinson & Dalton, 1979; Robinson et al., 1985).

$$\dot{\chi} = -i[\mathcal{H},\chi] - \Gamma_R\chi - \Gamma_\Omega\chi - i[\mathcal{H},\sigma_{eq}] \quad (1)$$

The density matrix at thermal equilibrium is given by $\sigma_{eq} = \exp\{-\mathcal{H}_0/k_BT\}$. The Hamiltonian, $\mathcal{H} = \mathcal{H}_0 + \epsilon(t)$, includes the orientation-dependent interactions of the electron spin ($\vec{S}$) with the magnetic field ($\vec{H}$) through the g-tensor and the electron spin with the nitrogen spin ($\vec{I}$) through the A-tensor

$$\mathcal{H}_0 = (\gamma_e/\bar{g})\vec{H}\cdot\mathbf{g}\cdot\vec{S} + \gamma_e\vec{I}\cdot\mathbf{A}\cdot\vec{S} \quad (2)$$

plus the interaction of the electron spin with the microwave field

$$\epsilon(t) = \gamma_e h_1 S_\pm e^{\mp i\omega t} \quad (3)$$

where γ_e is the electron gyromagnetic ratio, $\bar{g} = {}^1/_3$ Tr {g} is the isotropic g-factor, h_1 is the microwave field amplitude, and ω is the microwave radiation frequency, approximately 9 GHz at X band.

Full treatment of this equation for the case of duplex DNA would require a complete specification of all motional processes, which include the independent motion of the probe and the local motion of the base to which it is attached, the

internal collective motions of the base pairs, and the overall uniform tumbling motion of the duplex. Much progress has been made in specifying the correlation functions for this problem and in directly computing trajectories by Brownian dynamics simulations (Allison, 1986). Recently (Robinson et al., 1992), classical trajectories have been used to directly simulate CW-EPR spectra. However, in the present work, only the overall tumbling motion is treated explicitly in the stochastic Liouville equation. All internal motions are treated in the fast motion limit as discussed below.

The simulation program used to solve the stochastic Liouville equation has been described elsewhere (Robinson et al., 1985; Beth & Robinson, 1989). The simulations require the homogeneous spin–spin dephasing time for the electron (T_{2e}), the **A**- and **g**-tensor elements (partially averaged by internal motions), the diffusion tensor (**D**), and the tilt angles (Θ_{tilt} and Ψ_{tilt}) which determine the relative orientation of the diffusion tensor to the spin tensors. The **A**- and **g**-tensors are coincident. The principal, or z, component of the spin tensors is along the p_z orbital of the nitrogen and the x direction is taken to be along the N–O bond (Lajzerowicz-Bonneteau, 1976). A postcalculation Gaussian convolution is used to compensate for the superhyperfine splittings due to nuclear spins other than the nitroxide nitrogen.

Modeling Global Tumbling. For the purpose of modeling the global tumbling, a right circular cylinder can be taken as a reasonable approximation to a DNA duplex. The motional operator for axial, rigid body, Brownian diffusion is

$$\Gamma_\Omega = -\nabla\cdot\mathbf{D}\cdot\nabla \tag{4}$$

where the diffusion tensor in the principal axis frame of the molecule is given by

$$\mathbf{D} = \begin{pmatrix} D_{perp} & 0 & 0 \\ 0 & D_{perp} & 0 \\ 0 & 0 & D_{para} \end{pmatrix} \tag{5}$$

The Stokes–Einstein diffusion coefficients, D_{perp} and D_{para}, govern rotational motion perpendicular to and about the helix axis, respectively. The values of the diffusion coefficients for a right circular cylinder of length L and radius R are predicted by Tirado and de la Torre (1980) to be

$$D_{perp} = \frac{3kT\{\ln(p) + \delta_{perp}\}}{\pi\eta L^3} \tag{6}$$

$$D_{para} = \frac{kT}{(1 + \delta_{para})A\pi\eta LR^2} \tag{7}$$

where

$$p = L/2R$$

and $A = 3.841$, k is the Boltzmann constant, T is the absolute temperature, and η is the solvent viscosity. The viscosity of the buffer at a given temperature was assumed to be that of pure water (*CRC Handbook of Chemistry and Physics*, 1986). The viscosities of the sucrose solutions were calculated according to Barber (1966).

For duplex DNA, we have assumed $R = 12.0$ Å and $L = (3.4)N$ Å, where N is the number of base pairs (Wu et al., 1987). We have parametrized the values given by Tirado and de la Torre (1980) for the end-effect correction factors δ_{perp} and δ_{para} as follows:

$$\delta_{perp} = -0.662 + 0.913/p - 0.042/p^2 \tag{8}$$

$$\delta_{para} = +0.689/p - 0.203/p^2 \tag{9}$$

While Tirado and de la Torre give no results for $p < 2$, we have used eqs 8 and 9 to extend their results to the case of the 12 base pair duplex ($p = 1.7$) and obtained simulations which are in good agreement with the experimental EPR spectra. Eimer et al. (1990) have used a nearly identical parametrization and have extended the application to DNA duplexes as short as 8 base pairs.

The diffusion tensor is not necessarily coincident with the frame defined by the spin tensors. An Euler angle rotation is used to express the diffusion tensor in the frame of the spin tensors:

$$\mathbf{D}'(\Psi_{tilt},\Theta_{tilt},\Phi_{tilt}) = \mathbf{R}(\Psi_{tilt},\Theta_{tilt},\Phi_{tilt})\cdot\mathbf{D}\cdot\mathbf{R}^{-1}(\Psi_{tilt},\Theta_{tilt},\Phi_{tilt}) \tag{10}$$

where the rotation operator, **R**, is defined in the Appendix. Because of the cylindrical symmetry of the DNA helix, Φ_{tilt} has no bearing on the problem and is fixed to be zero. The angle between the z-axis of the spin tensors and the helix axis is given by Θ_{tilt}. For $\Psi_{tilt} = 0°$ the y-axis of the nitroxide remains perpendicular to the helix axis; for $\Psi_{tilt} = 90°$ the x-axis of the nitroxide is perpendicular to the helix axis.

Modeling the Internal Dynamics. The internal dynamics of spin-labeled DNA have been treated here in the fast motion limit. In this limit, a motionally averaged, effective set of **A**- and **g**-tensors which include the effect of the rapid internal dynamics on the EPR spectrum can be calculated (McConnell, 1976; Griffith & Jost, 1976). In the absence of any other motion (such as the global tumbling of the DNA), the resulting EPR spectrum would appear to be a rigid limit spectrum corresponding to the motionally averaged tensors.

A random motional process is considered to be fast if $\Delta\tau_c < 1$, where τ_c is the correlation time of the random motion and Δ is the width of the distribution of anisotropic magnetic interactions which are averaged by the motion (Nordio, 1976). For a random motion which fully decorrelates the orientation of the molecule (such as isotropic rotational diffusion), Δ is the full orientation-dependent frequency range of a given manifold in the EPR spectrum. For nitroxide spin-labels at X band:

$$\Delta \approx A_{zz} - {}^1/_2(A_{xx} + A_{yy}) \tag{11}$$

which gives $\tau_c \approx 1$ ns as the upper bound for the fast motion limit. Here, however, we are considering *limited-amplitude* motions which do not fully decorrelate the orientation of the molecule. In this case Δ should be limited to the range of anisotropic interactions which are decorrelated by the internal dynamics. This will raise the upper bound on τ_c and increase the validity of the assumption that all internal dynamics are in the fast motion limit.

Wu et al. (1987) have estimated the relaxation times of the slowest bending modes for 43 and 69 base pair duplexes to be 0.7 and 3.2 ns, respectively, assuming a dynamic persistence length of 500 Å. The mean-squared amplitude of deformation of a given base pair is given below in eq 19. The factors Q_{il}^2 (eq 22) give the contribution of the lth bending mode to the motion of the ith base pair. The contribution of the slowest bending mode, $l = 2$, to the motion of the base pair at the center of a duplex with an odd number of base pairs is precisely zero. That is, $Q_{il=2}^2 = 0$, if $i = (N + 1)/2$ for odd N. The duplexes in this study correspond very nearly to this situation, having an even number of base pairs with the labeled base at $i = (N + 2)/2$. In this case the contribution of the slowest bending mode to its motion should still be very small. The

next slowest mode, $l = 4$, which can contribute significantly to the motion of the central bases was estimated by Wu et al. (1987) to have decay constants of 0.124 and 0.472 ns for a 43 and 69 base pair duplex, respectively, well within the fast motion limit. These relaxation times will increase rapidly with N, being approximately proportional to N^4 (Song & Schurr, 1990), and will thus be larger in the case of the 96 base pair duplex included in this study. On the other hand, the relaxation times decrease linearly with the dynamic persistence length for which the choice of 500 Å is low (Song & Schurr, 1990; Fujimoto & Schurr, 1990; Schurr et al., 1992).

Two models of the internal dynamics have been developed in detail in the Appendix, limited-amplitude rotation about a single axis and limited-amplitude rotations about two orthogonal axes. Approximations to the results for both models have been developed such that a single set of equations can be used for either model. The motionally averaged tensors are determined by a single parameter, $\langle\phi'^2\rangle_{total}$, the total mean-squared amplitude of all internal motions. From eqs 57 and 45 in the Appendix:

$$\begin{aligned}
\bar{A}_{xx} &= A_{xx} + {}^1/_2\langle\phi'^2\rangle_{total}(A_{zz} - A_{perp}) \\
\bar{A}_{yy} &= A_{yy} + {}^1/_2\langle\phi'^2\rangle_{total}(A_{zz} - A_{perp}) \\
\bar{A}_{zz} &= A_{zz} - \langle\phi'^2\rangle_{total}(A_{zz} - A_{perp}) \\
\bar{g}_{xx} &= g_{xx} + {}^1/_2\langle\phi'^2\rangle_{total}(g_{zz} - g_{perp}) \\
\bar{g}_{yy} &= g_{yy} + {}^1/_2\langle\phi'^2\rangle_{total}(g_{zz} - g_{perp}) \\
\bar{g}_{zz} &= g_{zz} - \langle\phi'^2\rangle_{total}(g_{zz} - g_{perp}) \qquad (12)
\end{aligned}$$

where

$$\begin{aligned}
A_{perp} &= {}^1/_2(A_{xx} + A_{yy}) \\
g_{perp} &= {}^1/_2(g_{xx} + g_{yy})
\end{aligned}$$

These equations can be related to the order parameter, S, defined as (Griffith & Jost, 1976; Lipari & Szabo, 1980)

$$S = {}^1/_2(3\langle\cos^2\phi'\rangle_{total} - 1) \approx 1 - {}^3/_2\langle\phi'^2\rangle_{total}$$

where the approximation is valid for small amplitudes of oscillation. From eq 12, above, one may take the appropriate linear combination to obtain

$$\bar{A}_{zz} - {}^1/_2(\bar{A}_{xx} + \bar{A}_{yy}) = (A_{zz} - A_{perp})(1 - {}^3/_2\langle\phi'^2\rangle_{total})$$

which can be rearranged to give

$$\frac{\bar{A}_{zz} - {}^1/_2(\bar{A}_{xx} + \bar{A}_{yy})}{A_{zz} - A_{perp}} = \frac{\bar{A}_{zz} - \bar{a}}{A_{zz} - \bar{a}} = 1 - {}^3/_2\langle\phi'^2\rangle_{total} \approx S$$

which is equivalent to eq 35 of Griffith and Jost (1976) and to eq 2 of Steinhoff et al. (1989) assuming that the traces of A and $\bar{A}$ are both equal to $3\bar{a}$.

As noted above, our analysis does not include the relaxation times of the internal modes. Lipari and Szabo (1982a,b) have developed a "model-free" approach for the interpretation of NMR relaxation data. In their model the internal motion is characterized by a single relaxation time and an order parameter. The external or overall tumbling of the molecule is characterized by anisotropic rigid-body motion. From this model, a correlation function for the effects of the dynamics is constructed (Lipari & Szabo, 1982a). The linewidth data are then related to the correlation function through the associated spectral density functions. While this procedure can be used to interpret high-resolution NMR data (Lipari & Szabo, 1982b), it is inapplicable to the EPR data presented here because the overall tumbling of the DNA is too slow to cause the EPR spectra to be characterized as a series of well-defined Lorentzian lines.

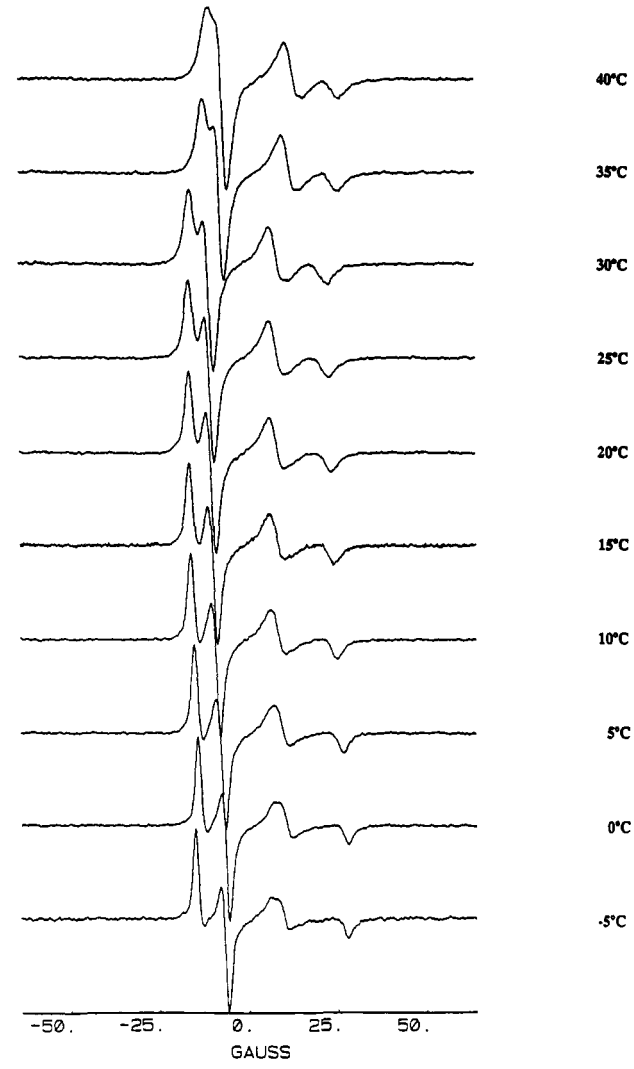

FIGURE 1: CW-EPR spectra of [^{15}N,D$_{13}$]-spin-labeled 24 base pair DNA duplex as a function of temperature.

RESULTS

Spectral Responses to Temperature and DNA Duplex Length. We have measured the EPR spectra of each of the four different DNA duplexes (Table I) as a function of temperature (from 0 to 40 °C) using both the naturally abundant [^{14}N,H$_{13}$]- and the isotopically substituted [^{15}N,D$_{13}$]-nitroxide spin-labels. Figure 1 shows, as a representative example, the temperature dependence of the EPR spectrum of the 24 base pair [^{15}N,D$_{13}$] spin-labeled duplex. The change in temperature from 0 to 40 °C corresponds to a increase in T/η, and thus the diffusion coefficients for uniform tumbling, D_{perp} and D_{para}, increase by a factor of 3.14. This set of spectra shows how the increase in the rate of motion causes the low-field manifold to collapse into a single averaged line. The x- and y-turning points of the high-field manifold are almost resolved at the lower temperatures, but are averaged out at the higher temperatures.

Figure 2 shows the EPR spectra of the four DNA duplexes at $T = 0$ °C using both the [^{14}N,H$_{13}$] and [^{15}N,D$_{13}$] spin-labels. These spectra clearly demonstrate that there is great

FIGURE 2: CW-EPR spectra (dotted lines) of 12, 24, 48, and 96 base pair DNA duplexes (from top to bottom) at $T = 0$ °C using both the [^{14}N,H$_{13}$] (right column) and the isotopically substituted [^{15}N,D$_{13}$] (left column) spin-labels. Simulations (solid lines) are overlaid on each spectrum.

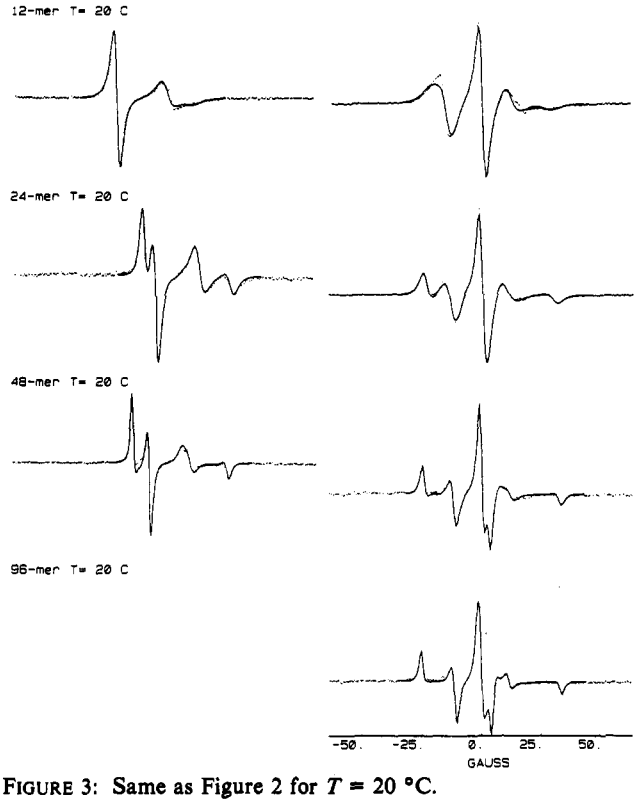

FIGURE 3: Same as Figure 2 for $T = 20$ °C.

sensitivity to the duplex length. The changes in the EPR line shapes are primarily due to the length dependence of the overall tumbling of the DNA. Figures 3 and 4 show analogous spectra at $T = 20$ °C and $T = 40$ °C, respectively. The dashed lines, superimposed on the experimental data, are the best fit

FIGURE 4: Same as Figure 2 for $T = 40$ °C.

simulations as discussed below. To simulate these spectra and determine the total mean-squared amplitude of internal motion, $\langle\phi'^2\rangle_{total}$, as a function of N, T, and η, it is first necessary to determine the rigid-limit **A**- and **g**-tensors and the orientation of these spin tensors to the diffusion tensor as determined by Θ_{tilt} and Ψ_{tilt}.

The Rigid-Limit Tensors. The set of DNA duplexes considered in this study all place the spin-label in the same local environment, i.e., near the center of the identical 12 base sequence. Therefore, it is reasonable to assume that there exists a single set of rigid-limit **A**- and **g**-tensors common to all the sequences considered in this study. However, finding a set of tensors which truly represents the no-motion limit is not a simple task. To determine the proper rigid-limit **A**- and **g**-tensors, it is necessary to slow, as much as possible, the motion of the spin-label. At the same time the conditions under which the rigid-limit spectrum is obtained should be as close as possible to the conditions under which all other experiments are performed. This is because the **A**- and **g**-tensors are somewhat solvent and environment dependent.

Figure 5 shows an overlay of the EPR spectra of the [^{14}N,H$_{13}$]-spin-labeled 24 and 48 base pair duplexes in 46% (w/w) sucrose buffer at 0 °C. In this high-viscosity solution, the global tumbling of the duplex is slowed to the extent that it is insignificant on the linear CW-EPR time scale. The estimated characteristic rotation times for the 48 base pair duplex in 46% sucrose buffer at 0 °C are $\tau_{para} = {}^1/_6 D_{para} = 375$ ns for motion about the helix axis and $\tau_{perp} = {}^1/_6 D_{perp} = 3950$ ns for end-over-end tumbling. The two spectra are virtually identical, indicating that the internal length-dependent motions have been damped, as well, such that they have no significant effect on the EPR spectra.

A comparison (not shown) of the EPR spectra of the [^{15}N,D$_{13}$]-spin-labeled 48 base pair duplex at 0 °C in 46% (w/w) and 51% (w/w) sucrose shows that the resulting increase in viscosity does slightly further slow the motion (presumably local) on the spin-label. Figure 6 shows the EPR spectrum

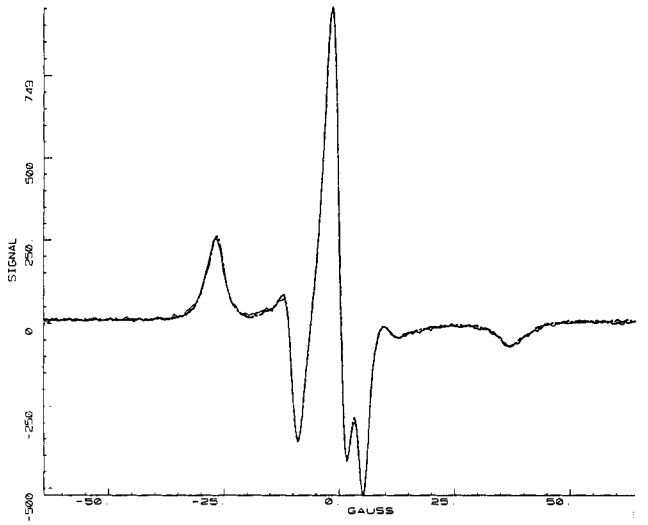

FIGURE 5: EPR spectrum of [^{14}N,H$_{13}$]-labeled 48-mer (solid line) overlaid with 24-mer (dashed line) both in 46% (w/w) sucrose pH = 7 buffer at 0 °C.

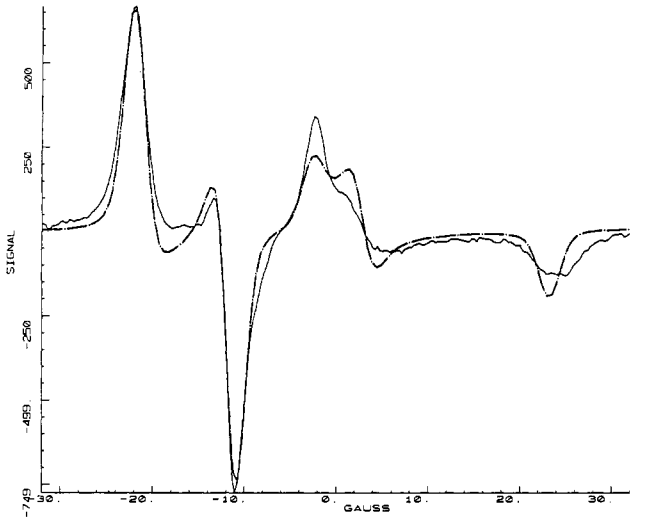

FIGURE 6: EPR spectrum (solid line) of [^{15}N,D$_{13}$] 48-mer in 51% (w/w) sucrose buffer at 0 °C with the rigid-limit simulation (dashed line) using the spin tensors in Table II. T_{2e} = 100 ns. The simulation was convolved with a 0.75-G Gaussian.

Table II: Rigid-Limit Tensor Elements for the [^{15}N,D$_{13}$]Spin-Label

A_{xx} (G)	A_{yy} (G)	A_{zz} (G)	g_{xx}	g_{yy}	g_{zz}
8.79	14.17	45.17	2.0076	2.00594	2.00290

of the [^{15}N,D$_{13}$]-spin-labeled 48 base pair duplex at 0 °C in 51% (w/w) sucrose overlaid with a rigid-limit simulation using the spin tensors given in Table II. The fit matches the turning points of the data quite well, although there is a some disagreement in the high-field region. The high-field extremum of the 51% sucrose spectrum has an unusually broad line shape. One possible interpretation of this feature is that the spin-label exists in at least two different internal conformations which are interconverting slowly (if at all) on the EPR time scale. If this is the case, then the tensors have been chosen to favor the component with the smaller value of A_{zz}.

To fit an EPR spectrum to a powder pattern, there are six major parameters which can be adjusted. These are the three components of the A-tensor (A_{xx}, A_{yy}, and A_{zz}) and the three components of the g-tensor (g_{xx}, g_{yy}, and g_{zz}). However, assuming that the isotropic value of the A-tensor ($\bar{a}$) is independent of the change in conditions on going from the near rigid limit to the fast motion limit, $\bar{a}$ can be obtained from spectra in the fast motion limit. From the EPR spectrum of [^{15}N,D$_{13}$]-spin-labeled thymine in buffer at 0 °C, a value of $\bar{a}$ = 22.71 G is obtained (Hustedt, 1989). The EPR spectrum of a nitroxide spin-label is relatively insensitive to the isotropic value of the g-tensor, $\bar{g}$. Hence, a reasonable value has been assumed, $\bar{g}$ = 2.00550, and will be used throughout. Thus, the number of independent parameters that need to be adjusted is reduced to four. Powder pattern simulations were performed using a program written by Balasubramanian and Dalton (1979).

The EPR spectrum in Figure 6 was chosen as the best estimate of the true rigid-limit spectrum. The A- and g-tensor elements for the simulation, optimized to within ±0.50 G and ±0.0001 uncertainty, respectively, are given in Table II. The tensors used for the [^{14}N,H$_{13}$] label are found from these tensors by multiplying the A-tensor elements for the [^{15}N,H$_{13}$] label by the ratio of the gyromagnetic ratios for the two spins, 0.7131. The g-tensor is taken to be the same for both spin-labels.

As the solvent polarity increases, a zwitterionic resonance structure with the unpaired spin density on the nitrogen is stabilized relative to a neutral resonance structure with spin density on the (spin zero) oxygen. The higher spin density on the nitrogen in a more polar solvent results in an increase in the value of $\bar{a}$ and A_{zz} (Morrisett, 1976). Hydrogen-bonding to the nitroxide oxygen also stabilizes charge on oxygen and increases $\bar{a}$ and A_{zz}. Hwang et al. (1975) observed two components in a low-temperature rigid-limit spectrum of perdeuterated tempone in ethanol-d_6. This result was interpreted as evidence of separate populations of hydrogen-bonded and non-hydrogen-bonded nitroxides in slow exchange. Johnson (1981) observed a temperature dependence of the spectral width (the distance in gauss between the z-turning points of the high- and low-field manifolds), $2A_{zz}^{obs}$, of both spin-labeled hemoglobin and fatty acid spin-labels in lipid bilayers. The temperature dependence of $2A_{zz}^{obs}$ was attributed to an equilibrium between hydrogen-bonded and non-hydrogen-bonded states with rapid exchange between the two states resulting in an average value of $2A_{zz}^{obs}$.

On the basis of the results of Hwang et al. (1975) and Johnson (1981), it is expected that the nitroxide of spin-labeled DNA may also form hydrogen-bonded complexes when immobilized. The possibility of hydrogen bond formation poses a considerable dilemma. On the one hand, to obtain the true rigid-limit spectrum it is desirable to lower the temperature of the sample to eliminate motion of the spin-label. On the other hand, reducing the temperature favors the formation of the hydrogen-bonded structure which has a different set of tensors. In the course of this work, EPR spectra of a sample of lyophilized [^{14}N,H$_{13}$]-labeled duplex DNA were obtained. This sample gave by far the largest $2A_{zz}^{obs}$ of all those studied. It seems likely that this is a result of the nitroxide being hydrogen bonded to residual H_2O in the sample. The measured value of $2A_{zz}^{obs} \approx 72.9$ G for the [^{14}N,H$_{13}$]-labeled lyophilized sample at T = −80 °C corresponds to $A_{zz} \approx 36.4$ G, which compares quite well with the value obtained by Hwang et al. for hydrogen-bonded tempone, 35.8 G (as compared to 33.5 G for the non-hydrogen-bonded form). Note that tempone is a 6-membered ring nitroxide, not the 5-membered ring used in these studies.

The EPR spectrum of the lyophilized [^{14}N,H$_{13}$]-labeled duplex DNA is nearly temperature independent over the range from 0 to −100 °C and never shows the unusual line shapes seen in Figure 2. The EPR spectra of spin-labeled duplex

DNA in high-viscosity solutions do change considerably over this temperature range. Furthermore, the lyophilized and high-viscosity samples give nearly identical results at low temperatures ($T \leq -80$ °C). These results suggest that there is an equilibrium between a hydrogen-bonded and a non-hydrogen-bonded form in the high-viscosity solutions. The nitroxide in the high-viscosity solution is essentilly 100% hydrogen bonded at −80 °C, while at $T = 0$ °C both forms exist and exchange between them is rather slow.

The extent to which residual motion in the spin-label in 51% sucrose at $T = 0$ °C or the equilibrium and exchange dynamics of multiple nitroxide environments influence the spectrum in Figure 6 is not yet fully resolved. Nevertheless, the EPR spectrum of the [^{15}N,D$_{13}$]-labeled T* 48 base pair duplex in 51% sucrose at 0 °C has been taken as the closest of all available data to the true rigid-limit spectrum. It is believed that these conditions strike the best possible compromise between slowing the dynamics of the spin-label and significantly changing the environment of the nitroxide.

Orientation of the Spin-Label to the Helix Axis. It is necessary to establish the orientation of the coincident A- and g-tensors of the spin-label relative to the axially symmetric rotational diffusion tensor of the DNA duplex. The largest splitting of the EPR spectrum in a nitroxide spin-label at X band is determined by A_{zz}. As a result, rotations which average A_{zz} into either A_{xx} or A_{yy} are the most important motional processes affecting the spectrum. The major tilt angle, Θ_{tilt}, determines whether global tumbling rotates the z-axis of the spin-label into the x–y plane at a rate governed by D_{perp} ($\Theta_{tilt} = 0°$) or D_{para} ($\Theta_{tilt} = 90°$). As previously demonstrated (Spaltenstein et al., 1989a; Hustedt, 1989), the EPR spectrum of a given duplex compares reasonably well to a simulation for a nitroxide undergoing isotropic rotation when the isotropic rotational correlation time is given by $^1/_6D_{perp}$. The success of this approach indicates that the motion of the z-axis of the nitroxide is primarily governed by D_{perp} and therefore Θ_{tilt} is small. The minor tilt angle, Ψ_{tilt}, interchanges A_{xx} and A_{yy}, which are approximately equal in comparison with A_{zz}. In fact, if the magnetic tensors are axial ($g_{xx} = g_{yy}$, $A_{xx} = A_{yy}$) or if $\Theta_{tilt} = 0°$, then the EPR spectrum is independent of Ψ_{tilt}. In the simulation program used, Θ_{tilt} can be freely adjusted while Ψ_{tilt} is constrained to be either 0° or 90°. For the reasons cited above, the simulations (in particular $2A_{zz}^{obs}$) are relatively insensitive to Ψ_{tilt} and only small errors are expected in the interior regions of the spectra as a result of the inability to freely vary Ψ_{tilt}.

The optimal value of Θ_{tilt} was determined by comparing simulations to the EPR spectrum of the [^{15}N,D$_{13}$]-labeled T* 48 base pair duplex at 0 °C. This spectrum was chosen because of the large anisotropy of the diffusion tensor and the well-resolved x- and y-turning points in the high-field line. Figure 7 shows the experimental spectrum overlaid with the simulations for $\Theta_{tilt} = 0°$, 20°, and 40° with $\Psi_{tilt} = 0°$. The A- and g-tensors used correspond to $\langle\phi'^2\rangle_{total} = 0.0512$. Larger values of Θ_{tilt} were tried and are clearly incorrect. Focusing on the x- and y-turning points of the high-field line, it appears that $\Theta_{tilt} = 20°$ is the best value. $\Theta_{tilt} = 0°$ clearly collapses the x- and y-turning points of the high-field manifold too much, while $\Theta_{tilt} = 40°$ does not collapse them enough. Simulations were also performed for other values of $\langle\phi'^2\rangle_{total}$. While both $\langle\phi'^2\rangle_{total}$ and Θ_{tilt} determine the $2A_{zz}^{obs}$ splitting of a given simulation, the fit to the x- and y-turning points of the high-field manifold is optimal for $\Theta_{tilt} = 20°$ independent of $\langle\phi'^2\rangle_{total}$.

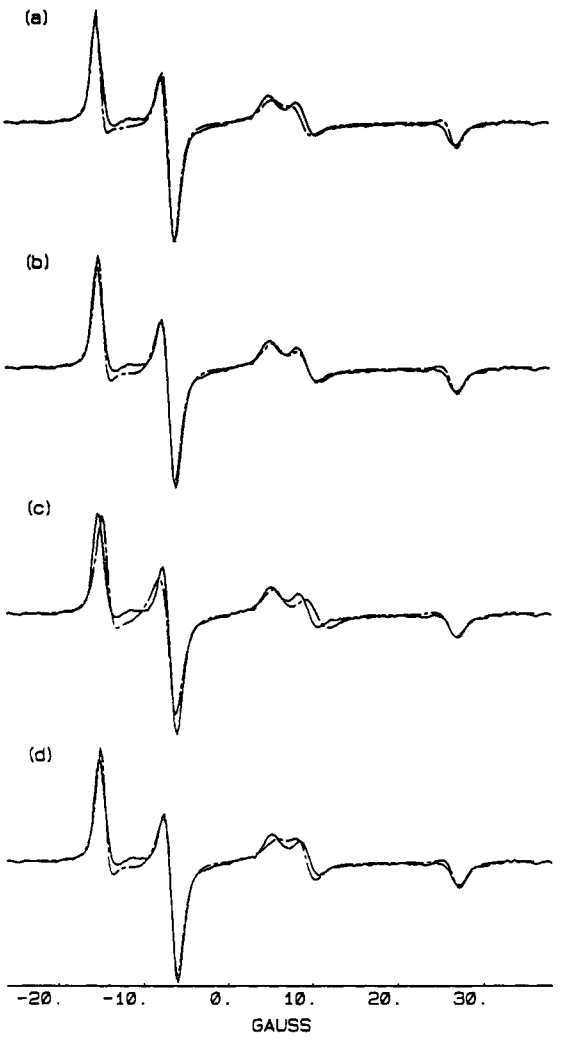

FIGURE 7: Simulation of the EPR spectrum of the [^{15}N,D$_{13}$]-spin-labeled 48 base pair duplex in buffer. Tensors were calculated according to eqs 12 for $\langle\phi'^2\rangle_{total} = 0.0512$. Characteristic rotational times were $1/(6D_{perp}) = 259$ ns and $1/(6D_{para}) = 24.6$ ns. Values of the two tilt angles are as follows: (a) $\Theta_{tilt} = 0°$, $\Psi_{tilt} = 0°$; (b) $\Theta_{tilt} = 20°$, $\Psi_{tilt} = 0°$; (c) $\Theta_{tilt} = 40°$, $\Psi_{tilt} = 0°$; (d) $\Theta_{tilt} = 20°$, $\Psi_{tilt} = 90°$.

Figure 7d shows the overlay of the same experimental spectrum with a simulation using $\Theta_{tilt} = 20°$ and $\Psi_{tilt} = 90°$ and can be compared to Figure 7B for which $\Theta_{tilt} = 20°$ and $\Psi_{tilt} = 0°$. The agreement is clearly better using $\Psi_{tilt} = 0°$ rather than $\Psi_{tilt} = 90°$. Thus, the optimal value of Ψ_{tilt} is close to 0°, but may be somewhat larger.

Simulations. The above results complete the prescription for simulating the EPR spectra of the spin-labeled DNA duplexes as a function of N, T, and η. The rigid-limit tensor values are given in Table II. Equations 12 generate, for a given value of $\langle\phi'^2\rangle_{total}$, the spin tensors averaged by the rapid internal motion. The roational diffusion coefficients for the global tumbling are determined by eqs 6 and 7. The tilt angles were set to $\Theta_{tilt} = 20°$ and $\Psi_{tilt} = 0°$. There is only one adjustable parameter, $\langle\phi'^2\rangle_{total}$, which is a direct measure of the amplitude of internal motion. The sole criterion used to determine $\langle\phi'^2\rangle_{total}$ was the match of the spectral width of the simulation, $2A_{zz}^{sim}$, to that of the data, $2A_{zz}^{obs}$. All other parameters being held fixed, $2A_{zz}^{sim}$ is a function of $\bar{A}_{zz}$ which is determined, in turn, by $\langle\phi'^2\rangle_{total}$. The best simulations of the EPR spectra of the four duplexes in buffer are overlaid on the data in Figures 2–4. The values of $\langle\phi'^2\rangle_{total}$ used to generate the simulations of the EPR spectra of the four

Table III: The Total Amplitude of Internal Motion, $\langle\phi'^2\rangle_{total}$

N	T (°C)	isotope	% sucrose	$\langle\phi'^2\rangle_{total}$ (rad^2)
12	0	^{15}N	0	0.0420
12	0	^{14}N	0	0.0332
24	0	^{15}N	0	0.0465
24	0	^{14}N	0	0.0377
48	0	^{15}N	0	0.0512
48	0	^{14}N	0	0.0512
96	0	^{14}N	0	0.0556
12	20	^{15}N	0	0.0733
12	20	^{14}N	0	0.0733
24	20	^{15}N	0	0.0750
24	20	^{14}N	0	0.0733
48	20	^{15}N	0	0.0778
48	20	^{14}N	0	0.0778
96	20	^{14}N	0	0.0866
12	40	^{15}N	0	0.1091
12	40	^{14}N	0	0.1091
24	40	^{15}N	0	0.1060
24	40	^{14}N	0	0.1091
48	40	^{15}N	0	0.1091
48	40	^{14}N	0	0.1133
96	40	^{14}N	0	0.1225
24	0	^{15}N	20	0.0333
24	0	^{14}N	20	0.0333
48	0	^{15}N	20	0.0420
12	0	^{15}N	35	0.0210
48	0	^{15}N	35	0.0377
24	20	^{15}N	20	0.0688
24	20	^{14}N	20	0.0734
48	20	^{15}N	20	0.0734
12	20	^{15}N	35	0.0377
48	20	^{15}N	35	0.0734
24	40	^{15}N	20	0.0960
24	40	^{14}N	20	0.1000
48	40	^{15}N	20	0.1046
12	40	^{15}N	35	0.0688
48	40	^{15}N	35	0.1046

duplexes in buffer are given in Table III and plotted in Figure 8. In the case of the 12 base pair duplex in buffer at 20 and 40 °C, the uniform mode has collapsed the line shape such that $2A_{zz}^{obs}$ cannot be measured. Furthermore, the simulations for these two spectra are largely insensitive to the value of $\langle\phi'^2\rangle_{total}$. The values of $\langle\phi'^2\rangle_{total}$ given in Table III for the 12 base pair duplex in buffer at 20 and 40 °C are those used for the simulations in Figures 3 and 4, but cannot be considered to be best fit estimates and are not included in the following analysis. The EPR spectra of selected spin-labeled duplexes were also measured at elevated viscosity using 20% and 35% (w/w) sucrose buffer solutions. The values of $\langle\phi'^2\rangle_{total}$ obtained from the simulations of these spectra are also given in Table III. It is apparent that $\langle\phi'^2\rangle_{total}$ is strongly temperature dependent but somewhat less dependent on viscosity, which is consistent with the interpretation of $\langle\phi'^2\rangle_{total}$ as being a measure of *internal* motion.

In overlaying a simulation on an experimental spectrum, a base-line shift and a scale factor have been used. These factors account for effects which are purely instrumental and have no physical significance. In each case the appropriate base line, b_y, and scale factor, s_y, were determined by minimizing the variance, σ^2, with respect to both b_y and s_y.

$$\sigma^2 = \sum_{n=1}^{M}(Y_n - b_y - s_y Y'_n)^2/M \qquad (13)$$

where Y_n are the data points, Y'_n are the simulation points, and M is the total number of points in each. The optimal

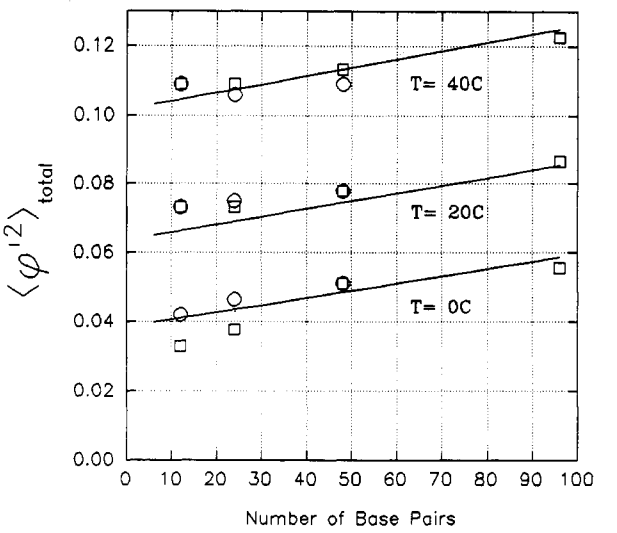

FIGURE 8: Plot of values of $\langle\phi'^2\rangle_{total}$ as a function of the number of base pairs, N, at T = 0 °C, T = 20 °C, and T = 40 °C for both the [^{15}N,D$_{13}$] spin-label (open circles) and the [^{14}N,H$_{13}$]-spin-labeled (open squares) DNA duplexes in buffer. The data are given in Table III, and only those for 0% sucrose are used. The solid lines of increasing height were calculated from eq 31 using $f(T)$ from eq 27, q = 7.1, and $(m \pm \sigma_m) = (2.27 \pm 0.30) \times 10^{-4}$ and $(b \pm \sigma_b) = (6.36 \pm 0.015) \times 10^{-2}$ rad^2. The least-squares fits were obtained using all of the data in the figure except for the 12 base pair duplex at 20 and 40 °C. The data corresponding to a given temperature lie closest to their respective fits.

values of s_y and b_y are given by

$$s_y = \sum_{n=1}^{M}(Y_n - \bar{Y})(Y'_n - \bar{Y}') \Big/ \sum_{n=1}^{M}(Y'_n - \bar{Y}')(Y'_n - \bar{Y}') \qquad (14)$$

and

$$b_y = \bar{Y} - s_y\bar{Y}' \qquad (15)$$

where

$$\bar{Y} = \frac{1}{M}\sum_{n=1}^{M} Y_n$$

and

$$\bar{Y}' = \frac{1}{M}\sum_{n=1}^{M} Y'_n$$

are the mean values of the data and simulation, respectively. When the above expressions for s_y and b_y are substituted back into the eq 13, then σ^2 can be written as

$$\sigma^2 = \frac{(1-R^2)}{M}\sum_{n=1}^{M}(Y_n - \bar{Y})^2 \qquad (16)$$

where the correlation coefficient (Edwards, 1969), R, is defined as

$$R = \frac{\sum_{n=1}^{M}(Y_n - \bar{Y})(Y'_n - \bar{Y}')}{\left[\sum_{n=1}^{M}(Y_n - \bar{Y})^2 \sum_{n=1}^{M}(Y'_n - \bar{Y}')^2\right]^{1/2}} \qquad (17)$$

R is bounded by the Schwarz inequality, $-1 \le R \le +1$, and is a dimensionless way to represent the variance between the simulation and the data. Maximizing R is equivalent to

minimizing σ^2. In all of the simulations shown in Figures 2–4, $R > 0.98$ has been achieved.

DISCUSSION

The results in Figure 8 show the expected trends. The value of $\langle\phi'^2\rangle_{total}$ clearly increases as a function of both duplex length and temperature. Overlaid on the data in Figure 8 are fits obtained by modeling the duplex as a weakly bending rod as suggested by Schurr (personal communication). In general, the mean-squared amplitudes of independent motional processes are additive. Therefore, the total mean-squared amplitude of internal motion is equal to the sum of the total length-independent motion, $\langle\xi^2\rangle_{total}$, and the length-dependent motion, $\langle\eta^2\rangle_{total}$:

$$\langle\phi'^2\rangle_{total} = \langle\xi^2\rangle_{total} + \langle\eta^2\rangle_{total} \tag{18}$$

Because the z-axis of the spin-label is nearly aligned with the helix axis, the T* probe is primarily sensitive to flexural as opposed to torsional motions. We suggest that the length-dependent internal motions are due exclusively to the collective bending motions of the DNA. Wu et al. (1987) have described how flexural deformations of a weakly bending rod induce local fluctuations. The mean-squared angular displacement of the ith base pair in the y–z plane of the helix is related to the dynamic flexural persistence length, P_{df}, by

$$\langle[\eta_i(\infty) - \eta_i(0)]^2\rangle = 2\sum_{l\geq 2}^{N} Q_{il}^2 d_l^2 \tag{19}$$

where

$$d_l^2 = \frac{h}{P_{df}\Lambda_l} \tag{20}$$

$$\Lambda_l = 4\sin^2\left\{\frac{(l-1)\pi}{2N}\right\} \tag{21}$$

$$Q_{il}^2 = \frac{2}{N}\cos^2\left\{\frac{(i-1/2)(l-1)\pi}{N}\right\} \tag{22}$$

Here, d_l^2 is the mean-squared amplitude of lth bending mode and Q_{il}^2 gives the contribution of the lth mode to the motion of the ith base pair.

The sum in eq 19 has an analytic solution (Allison & Schurr, 1979):

$$\langle\eta_i^2(\infty) - \eta_i^2(0)\rangle = 2\sum_{l\geq 2}^{N} Q_{il}^2 d_l^2 = \frac{Nh}{6P_{df}}\left\{1 + 3\left[\frac{2i-N-1}{N}\right]^2\right\} \tag{23}$$

where $h = 3.4$ Å is the distance between base pairs. For the duplexes studied here the spin-label is attached to the $[i = (N + 2)/2]$-th base pair, where N is even. The length-dependent motion is assumed to be two dimensional and isotropic with mean-squared amplitude of $\langle\eta^2\rangle$ in either direction.

$$\begin{aligned}\langle\eta^2\rangle_{total} &= 2\langle\eta^2\rangle = \langle[\eta_i(\infty) - \eta_i(0)]^2\rangle \\ &= \langle[\eta_i(\infty)^2 - 2\eta_i(\infty)\eta_i(0) + \eta_i(0)^2]\rangle \\ &= 2\langle\eta_i(0)^2\rangle \\ &= \frac{h}{6P_{df}}\left(N + \frac{3}{N}\right)\end{aligned} \tag{24}$$

Wilcoxon and Schurr (1983) have shown that the persistence length is either independent of T if the bending angle between two adjacent base pairs is governed by a square-well potential or inversely proportional to T if the bending angle is governed by a harmonic potential. Thus the dynamic persistence length can be written as

$$P_{df}(T) = P_{df}(T = 293\text{ K}) \times f(T) \tag{25}$$

where

$$f(T) = 1 \tag{26}$$

for a square-well local bending potential and

$$f(T) = \frac{(293\text{ K})}{T} \tag{27}$$

for a harmonic potential. Therefore:

$$\langle\eta^2\rangle_{total} = \frac{h}{6P_{df}(T = 293\text{ K})}\frac{1}{f(T)}\left(N + \frac{3}{N}\right) \tag{28}$$

is nearly linear in N and may be linear in or independent of T.

There is no a priori reason to suspect that $\langle\xi^2\rangle_{total}$ is a simple function of temperature. We have assumed that the length-independent motion has a power law dependence on T:

$$\langle\xi^2\rangle_{total} = \langle\xi^2\rangle_{total}^{T=293K} g(q,T) \tag{29}$$

where

$$g(q,T) = \left(\frac{T}{293\text{ K}}\right)^q \tag{30}$$

for an unknown value of q.

The total mean-squared amplitude of internal motion is then given by

$$\langle\phi'^2\rangle_{total} = \frac{m}{f(T)}\left(N + \frac{3}{N}\right) + bg(q,T) \tag{31}$$

where

$$m = \frac{h}{6P_{df}(T = 293\text{ K})} \quad \text{and} \quad b = \langle\xi^2\rangle_{total}^{T=293K}$$

The data in Table III corresponding to the four duplexes in buffer (0% sucrose) were simultaneously fit by least-squares analysis to eq 31. Both forms of $f(T)$ (eqs 26 and 27) and various values of q were tested. The standard error of the fit was minimized when the dynamic persistence length was taken to be inversely proportional to temperature and $q = 7.1$ was used. In this case, $(m \pm \sigma_m) = (2.27 \pm 0.30) \times 10^{-4}$ and $(b \pm \sigma_b) = (6.36 \pm 0.015) \times 10^{-2}$ rads^2 were obtained.

Wilcoxon and Schurr (1983) concluded that they could not determine whether the dynamic persistence length was independent of temperature or inversely proportional to temperature. We have found a slight, but statistically insignificant, preference for the model in which the dynamic persistence length was inversely proportional to the T and likewise conclude that we are unable to distinguish between these two cases.

The value of m obtained corresponds to a *dynamic* flexural persistence length of 2500 ± 340 Å at 20 °C, where the error range is given by one standard deviation. This estimate of the *dynamic* flexural persistence length is about 5 times larger than the *static* persistence length, 500 Å (Schurr & Schmitz, 1986), and the *dynamic twisting* persistence length, 640 Å (Wilcoxon & Schurr, 1983). However, there is growing evidence that the dynamic flexural persistence length of DNA may be considerably larger than the static persistence length. Simulations by Allison et al. (1989) of the transient photodichroism of a 209 base pair duplex required a dynamic persistence length of at least 1000 Å. Song and Schurr (1990) have analyzed the transient electric dichroism data for DNA

fragments with 95–250 base pairs in low-salt conditions, 2 mM Na^+, and obtained a best fit using a dynamic persistence length 2100 Å. More recently, Schurr and co-workers have proposed that 1500 Å is the current best estimate of the dynamic persistence length (Fujimoto & Schurr, 1990; Schurr et al., 1992).

From $b = 0.0636$ and $q = 7.1$, the calculated total root-mean-squared amplitude, $(\langle\xi^2\rangle_{total})^{1/2}$, of the length-independent motion is 11.2 ± 0.2° at $T = 0$ °C, 14.5 ± 0.2° at 20 °C, and 18.2 ± 0.2° at 40 °C. These values can be taken to represent the amplitude of motion of the spin-label about the acetylenic tether. The value of $(\langle\xi^2\rangle_{total})^{1/2}$ increases strongly with temperature, which presumably represents a softening of the pocket in which the spin-label resides. On the other hand, if the length-independent motion is taken to be isotropic two-dimensional local wobble of the labeled base pair, then $\langle\xi^2\rangle_{total} = \langle\xi^2\rangle_x + \langle\xi^2\rangle_y = 2\langle\xi^2\rangle$ and the root-mean-squared amplitudes about either axis are 7.9°, 10.3°, and 12.9° at $T = 0$, 20, and 40 °C, respectively. This estimate is only slightly larger than the value of 7° obtained by Shibata et al. (1985) from the initial depolarization in FPA experiments.

Typically, the spin-labeling technique will overestimate (as opposed to underestimate) rates or amplitudes of motion because of the possibility of independent motion of the probe relative to the labeled molecule. It is clear from the data that the nature of the T* probe does not allow for any large-amplitude, independent motions of the spin-label. At $T = 0$ °C, the change in $\langle\phi'^2\rangle_{total}$ as a function of N is approximately 50% of the $N = 1$ value over the range studied. Thus there is considerable sensitivity to the length-dependent internal motions of the DNA as opposed to independent motion of the spin-label.

One possible source of systematic error is the choice of the rigid-limit tensors. We now demonstrate that errors in the rigid-limit tensor values do not have a large impact on the determined value of the persistence length: For each experimental spectrum, a value of $\bar{A}_{zz}$ was chosen such that, given the global tumbling of the duplex, the spectral width of the simulation, $2A_{zz}^{sim}$, matched the spectral width of the data, $2A_{zz}^{obs}$. The required value of $\bar{A}_{zz}$ depends only on the dynamics, D_{perp} and D_{para}, and the experimental data and does not depend on the rigid-limit tensors. The total mean-squared amplitude of internal motion is then determined by

$$\langle\phi'^2\rangle_{total} = \frac{A_{zz} - \bar{A}_{zz}}{A_{zz} - A_{perp}} \tag{32}$$

From eq 31, $\langle\phi'^2\rangle_{total}$ is approximately linear in N, the slope being proportional to the inverse of the persistence length. Thus

$$\frac{1}{P_{df}} \propto \frac{\partial\langle\phi'^2\rangle_{total}}{\partial N} = -\frac{\partial\bar{A}_{zz}}{\partial N}\frac{1}{A_{zz} - A_{perp}} \tag{33}$$

A 10% error in $A_{zz} - A_{perp}$ (which would be very large) gives a corresponding 10% error in P_{df}. We have already noted that the choice of $A_{zz} - A_{perp}$ is at the small end of the range of possible values, and an increase in $A_{zz} - A_{perp}$ would result in an *increase* in the persistence length.

CONCLUSIONS

The purity and homogeneity of the samples are reflected in the EPR spectra, which show neither contamination from secondary forms of the DNA (such as single strand) nor a broadening of the extrema of the spectra which would indicate a heterogeneity of spin-labeled sites. The T* probe provides a basis for conducting EPR studies on a variety of DNA duplexes. This work demonstrates the possibilities for the study of dynamics of specific sequences of duplex DNA. The ability of site-specifically label DNA allows direct comparisons of the data to theories of DNA dynamics (Barkley & Zimm, 1979; Robinson et al., 1980a,b; Allison & Schurr, 1979; Schurr, 1984) at a level of detail not easily obtained using nonspecific probes.

We have developed a means of approximately separating motion into overall tumbling and internal length-independent and internal length-dependent motions. The simulations demonstrate the accuracy of the theory for the rotational diffusion of a right circular cylinder and the applicability of that theory to DNA (Pecora, 1991). This suggests the possibility that EPR can be used to test more carefully the assumptions about the length and hydrodynamic radius used in the theory for the tumbling of a right circular cylinder.

The interpretation of $\langle\phi'^2\rangle_{total}$ is clearly model dependent. However, the assumption that mean-squared amplitudes of statistically independent processes are summable is well established in the statistical literature. Therefore, the separation of $\langle\phi'^2\rangle_{total}$ into length-dependent and a length-independent contributions seems quite reasonable. The length-dependent mean-squared amplitude of motion is proportional to N, as suggested by Wu et al. (1987). At X band, the probe is sensitive to bending, as opposed to twisting, motions of DNA. While our result for the dynamic persistence length is at the high end of the range of values determined by others, it is consistent with the notion that the dynamic persistence length is considerably larger than static persistence length (Allison et al., 1989; Fujimoto & Schurr, 1990; Song & Schurr, 1990; Schurr et al., 1992). It may well be that the presence of the spin-label locks out local motions of the DNA, but this would primarily affect the length-independent dynamics.

It has been assumed that the influence of torsional dynamics to the EPR spectra of T*-labeled DNA duplexes is negligible. All experiments were performed at X band (9 GHz). At this frequency, the EPR spectra are not strongly dependent on motions about the z-axis of the nitroxide. Since the optimum tilt angle is $\Theta_{tilt} = 20°$, the probe is primarily sensitive to the end-to-end uniform tumbling motion (D_{perp}) and internal bending motions. At higher microwave frequencies such as K-band (22 GHz) or Q-band (35 GHz), the influence of the highly nonaxial g-tensor is enhanced. With the increased x–y anisotropy there is increased sensitivity to rotations about the z-axis of the nitroxide (Beth and Robinson, 1989). Therefore, by scaling the frequencies at which the spectra are recorded, one can vary the contributions of flexural and torsional motions to the EPR spectrum of the duplex.

ACKNOWLEDGMENT

We are grateful for the assistance of J. Beltman, M. Tippie, F. Miyake, S. Ribero, and J. Millard without whom this work would not have progressed. We would like to thank Drs. J. M. Schurr, A. S. Benight, N. C. Seeman, and G. Drobny for their many helpful discussions and suggestions during the course of this work.

APPENDIX

Averaging the **A**- *and* **g**-*Tensors.* Van et al. (1974) have derived expressions for the effect of a limited-amplitude, rapid motion of nitroxide spin-labels. The following is based on the work of Van et al., but differs in that here an active, rather than passive, interpretation of the transformations is used

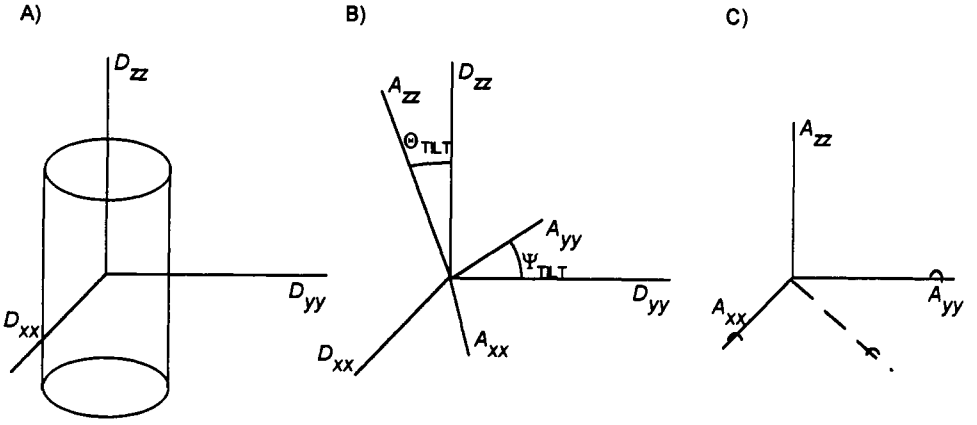

FIGURE 9: (A) Orientation of the rotational diffusion tensor ($D_{perp} = D_{xx} = D_{yy}$, $D_{para} = D_{zz}$) with respect to the DNA helix (the cylinder). (B) Orientation of the A- (and g-) tensors of the nitroxide (A_{xx}, A_{yy}, and A_{zz}) with respect to the rotational diffusion tensor of the DNA as determined by the angles Θ_{tilt} and Ψ_{tilt}. (C) Internal dynamics is modeled either as a limited-amplitude rotation about a single axis (dashed line) bisecting the x–y plane of the nitroxide or as simultaneous limited-amplitude rotations about the x- and y-axes of the nitroxide (A_{xx} and A_{yy}).

(Goldstein, 1980). In the following discussion, the A-tensor is considered; equivalent expressions for the g-tensor can be obtained by substituting g for A. For a nitroxide spin-label at the orientation at which its A and g-tensors are diagonal, let the A-tensor be given by $\mathbf{A}_d$. The A-tensor at any other orientation, $\mathbf{A}'(\psi,\theta,\phi)$, is given by an Euler angle rotation:

$$A'(\psi,\theta,\phi) = \mathbf{R}(\psi,\theta,\phi)\cdot\mathbf{A}_d\cdot\mathbf{R}^{-1}(\psi,\theta,\phi) \tag{34}$$

where the rotation operator is defined by

$$\mathbf{R}(\psi,\theta,\phi) = \mathbf{R}_\psi\mathbf{R}_\theta\mathbf{R}_\phi \tag{35}$$

$$\mathbf{R}_\psi = \begin{pmatrix} \cos\psi & \sin\psi & 0 \\ -\sin\psi & \cos\psi & 0 \\ 0 & 0 & 1 \end{pmatrix}$$

$$\mathbf{R}_\theta = \begin{pmatrix} \cos\theta & 0 & -\sin\theta \\ 0 & 1 & 0 \\ \sin\theta & 0 & \cos\theta \end{pmatrix}$$

$$\mathbf{R}_\phi = \begin{pmatrix} \cos\phi & \sin\phi & 0 \\ -\sin\phi & \cos\phi & 0 \\ 0 & 0 & 1 \end{pmatrix}$$

The rapid motions of interest here are complete or partial rotations about a given axis. The approach used is to orient the spin-label, via an Euler angle rotation, so that this axis of rapid rotation is aligned with the laboratory z-axis. In this case, the rotation corresponding to the angle ψ commutes with the subsequent rotation describing the rapid motion and has no bearing on the problem. Therefore, ψ can be set to zero. The individual elements of $\mathbf{A}'$ are given by

$$A'_{11} = A_{xx}\cos^2\theta\cos^2\phi + A_{yy}\cos^2\theta\sin^2\phi + A_{zz}\sin^2\theta$$

$$A'_{22} = A_{xx}\sin^2\phi + A_{yy}\cos^2\phi$$

$$A'_{33} = A_{xx}\sin^2\theta\cos^2\phi + A_{yy}\sin^2\theta\sin^2\phi + A_{zz}\cos^2\theta$$

$$A'_{12} = A'_{21} = -(A_{xx} - A_{yy})\cos\theta\cos\phi\sin\phi$$

$$A'_{13} = A'_{31} = (A_{xx}\cos^2\phi + A_{yy}\sin^2\phi - A_{zz})\cos\theta\sin\theta$$

$$A'_{23} = A'_{32} = -(A_{xx} - A_{yy})\sin\theta\cos\phi\sin\phi \tag{36}$$

where A_{xx}, A_{yy}, and A_{zz} are the three principal components of $\mathbf{A}_d$. The motion of the spin-label is described by a rotation of angle ϕ' about the z-axis, which gives

$$R_{\phi'}\cdot\mathbf{A}'\cdot R_{\phi'}^{-1} =$$

$$\begin{pmatrix} \left[\begin{matrix} A'_{11}\cos^2\phi' + \\ 2A'_{12}\cos\phi'\sin\phi' + \\ A'_{22}\sin^2\phi' \end{matrix}\right] & \left[\begin{matrix} -(A'_{11} - A'_{22})\cos\phi'\sin\phi' + \\ A'_{12}(\cos^2\phi' - \sin^2\phi') \end{matrix}\right] & \left[\begin{matrix} A'_{13}\cos\phi' + \\ A'_{23}\sin\phi' \end{matrix}\right] \\ \left[\begin{matrix} -(A'_{11} - A'_{22})\cos\phi'\sin\phi' + \\ A'_{12}(\cos^2\phi' - \sin^2\phi') \end{matrix}\right] & \left[\begin{matrix} A'_{11}\sin^2\phi' - \\ 2A'_{12}\cos\phi'\sin\phi' + \\ A'_{22}\cos^2\phi' \end{matrix}\right] & \left[\begin{matrix} -A'_{13}\sin\phi' + \\ A'_{23}\cos\phi' \end{matrix}\right] \\ \left[A'_{13}\cos\phi' + A'_{23}\sin\phi'\right] & \left[-A'_{13}\sin\phi' + A'_{23}\cos\phi'\right] & A'_{33} \end{pmatrix} \tag{37}$$

and the motionally averaged A-tensor is obtained by averaging the elements of this tensor over ϕ' through the desired range of motion:

$$\bar{\mathbf{A}}' = \langle R_{\phi'}\cdot\mathbf{A}'\cdot R_{\phi'}^{-1}\rangle_{\phi'} \tag{38}$$

We will consider two models, motional averaging about one axis of rotation and motional averaging about two perpendicular axes of rotation (see Figure 9).

Motional Averaging about One Axis of Rotation. The necessary averages of trigonometric functions are

$$\langle\cos\phi'\rangle = \int_{-\infty}^{\infty}\rho(\phi')\cos\phi'\,d\phi' = \beta$$

$$\langle\sin\phi'\rangle = \int_{-\infty}^{\infty}\rho(\phi')\sin\phi'\,d\phi' = 0$$

$$\langle\cos\phi'\sin\phi'\rangle = \int_{-\infty}^{\infty}\rho(\phi')\cos\phi\sin\phi'\,d\phi' = 0$$

$$\langle\cos^2\phi'\rangle = \int_{-\infty}^{\infty}\rho(\phi')\cos^2\phi'\,d\phi' = 1 - \alpha$$

$$\langle\sin^2\phi'\rangle = \int_{-\infty}^{\infty}\rho(\phi')\sin^2\phi'\,d\phi' = \alpha \tag{39}$$

where $\rho(\phi')$ is a symmetric, time-independent, normalized distribution function which characterizes the nature of the motion. For motion in a square-well potential, $\rho(\phi')$ is a uniform distribution over a limited range, $\pm\phi'_{max}$. For motion in a harmonic potential, $\rho(\phi')$ is a Guassian disitribution. The equation for α can be expanded as a power series in ϕ':

$$\alpha = \langle\sin^2\phi'\rangle = \langle(\phi' - \phi'^3/6 + \ldots)^2\rangle \tag{40}$$

which for small amplitudes of motion can be truncated after the first term:

$$\alpha \approx \langle\phi'^2\rangle \tag{41}$$

Thus, in the limit of a highly restricted rotation, α is equal to the mean-squared amplitude of motion.

The motionally averaged A-tensor for an arbitrary axis of rotation is

$$\bar{\mathbf{A}}' = \begin{pmatrix} (1-\alpha)A'_{11} + \alpha A'_{22} & (1-2\alpha)A'_{12} & \beta A'_{13} \\ (1-2\alpha)A'_{12} & \alpha A'_{11} + (1-\alpha)A'_{22} & \beta A'_{23} \\ \beta A'_{13} & \beta A'_{23} & A'_{33} \end{pmatrix} \tag{42}$$

In the limit of complete unrestricted rotation, $\alpha = {}^1/_2$, $\beta = 0$, and the resulting motionally averaged tensor is axial:

$$\bar{\mathbf{A}}' = \begin{pmatrix} {}^1/_2(A'_{11} + A'_{22}) & 0 & 0 \\ 0 & {}^1/_2(A'_{11} + A'_{22}) & 0 \\ 0 & 0 & A'_{33} \end{pmatrix} \tag{43}$$

It is important to note that the data presented here clearly preclude the use of a model of internal dynamics which produces axial tensors. The EPR spectra of the [^{15}N,D$_{13}$]-labeled 48 base pair duplex clearly show the splitting of the x- and y-turning points in the high-field manifold which are characteristic of nonaxial A- and g-tensors.

The most important motions to be considered are those which rotate A_{zz} into A_{xx} and A_{yy}. The effect of such motions will be to reduce the z-component of the motionally averaged A-tensor and consequently reduce the spectral width, $2A_{zz}^{obs}$. Rapid rotation about the axis defined by A_{zz} averages A_{xx} with A_{yy}, but does not change A_{zz}. This produces subtle changes in line shape, but leaves $2A_{zz}^{obs}$ unchanged. One potentially important source of motion in T* is rotation of the spin-label about the linear acetylenic tether independent of the base (Kirchner et al., 1990). As is evident from the chemical structure of T*, the acetylenic tether axis is perpendicular to the z-axis of the nitroxide and approximately bisects its x–y plane. The orientation required to model this motion is achieved by setting $\theta = 90°$ and $\phi = 45°$. The choice of $\phi = 45°$ is approximate and is made for mathematical convenience. Evaluating the elements of A′ at $\theta = 90°$ and $\phi = 45°$ and substituting into eq 42 gives

$$\bar{\mathbf{A}}' = \begin{pmatrix} (1-\alpha)A_{zz} + \alpha A_{perp} & 0 & 0 \\ 0 & \alpha A_{zz} + (1-\alpha)A_{perp} & -\beta A^* \\ 0 & -\beta A^* & A_{perp} \end{pmatrix} \tag{44}$$

where

$$A_{perp} = {}^1/_2(A_{xx} + A_{yy}) \text{ and } A^* = {}^1/_2(A_{xx} - A_{yy}) \tag{45}$$

Now, the motionally averaged tensor is rotated back to its original orientation, reversing the rotation of eq 34:

$$\bar{\mathbf{A}} = R^{-1}(0,90°,45°)\cdot\bar{\mathbf{A}}'\cdot R(0,90°,45°) = \begin{pmatrix} A_{perp} + \frac{\alpha}{2}(A_{zz} - A_{perp}) + \beta A^* & -\frac{\alpha}{2}(A_{zz} - A_{perp}) & 0 \\ -\frac{\alpha}{2}(A_{zz} - A_{perp}) & A_{perp} + \frac{\alpha}{2}(A_{zz} - A_{perp}) - \beta A^* & 0 \\ 0 & 0 & A_{zz} - \alpha(A_{zz} - A_{perp}) \end{pmatrix} \tag{46}$$

Note that $\bar{\mathbf{A}}$ is not diagonal, but can be diagonalized by a subsequent rotation about the z-axis. The angle of rotation required to diagonalize $\bar{\mathbf{A}}$ will depend on the three elements of the original A-tensor. If one considers the equivalent result for the g-tensor, it becomes evident that the angle of rotation required to diagonalize $\bar{\mathbf{g}}$ must be different than that for $\bar{\mathbf{A}}$. Thus, this motional model produces average A- and g-tensors whose x- and y-components are no longer coincident. The fact that the motionally averaged A- and g-tensors are not coincident will be ignored. The diagonalization does not alter the z-components of the tensors which do remain coincident. The three principal components of the diagonalized $\bar{\mathbf{A}}'$ are as follows:

$$\bar{A}_{xx} = A_{perp} + \frac{\alpha}{2}(A_{zz} - A_{perp}) - \left\{[\beta A^*]^2 + \left[\frac{\alpha}{2}(A_{zz} - A_{perp})\right]^2\right\}^{1/2}$$

$$\bar{A}_{yy} = A_{perp} + \frac{\alpha}{2}(A_{zz} - A_{perp}) + \left\{[\beta A^*]^2 + \left[\frac{\alpha}{2}(A_{zz} - A_{perp})\right]^2\right\}^{1/2}$$

$$\bar{A}_{zz} = A_{zz} - \alpha(A_{zz} - A_{perp}) \tag{47}$$

The value of the z-component is reduced by $\alpha(A_{zz} - A_{perp})$, while the x- and y-components of the motionally averaged A-tensor depend on both α and β. To calculate A_{xx} and A_{yy} requires specifying a particular motional model [i.e., a particular $\rho(\phi')$ in eqs 39], so that α and β can be simultaneously determined. In practice, we have found that, for motion in a square-well or harmonic potential, the approximation $\bar{A}^* = A^*$ is valid for small-amplitude motions. This gives

$$\bar{A}_{xx} = A_{perp} + \frac{\alpha}{2}(A_{zz} - A_{perp}) + A^*$$

$$\bar{A}_{yy} = A_{perp} + \frac{\alpha}{2}(A_{zz} - A_{perp}) - A^*$$

$$\bar{A}_{zz} = A_{zz} - \alpha(A_{zz} - A_{perp}) \tag{48}$$

With this approximation, the three components of $\bar{\mathbf{A}}$ depend only on the single parameter, α, and are not specific to a particular motional model. The approximation does not alter $\bar{A}_{zz}$, the component which is critical to the analysis of the internal dynamics of spin-labeled DNA.

Motional Averaging about Two Axes of Rotation. We consider now, as a model for the internal dynamics, independent motion about two axes, the x- and y-axes of the spin-label. Because the DNA helix axis and the z-axis of the nitroxide are nearly parallel, $\Theta_{tilt} = 20°$, these two motions serve as models for bending about the x- and y-axes of the DNA. Both are treated exactly as above with $\theta = 90°$ and $\phi = 0°$ corresponding to motion about the x-axis and $\theta = 90°$ and $\phi = 90°$ to motion about the y-axis. The order in which the two independent motions are considered does influence the final results. Calculations for the two possible orders were performed and these results averaged. It is assumed that the amplitude of motion about the two axes is the same.

A rotation of A_d is performed as defined in eq 34, with $\theta = 90°$ and $\phi = 0°$. The effect of motion, as defined in eq 38, is averaged according to the results in eqs 39 and 42. The resulting averaged tensor is then rotated back to its original

orientation, to give

$$\bar{\mathbf{A}} = \begin{pmatrix} A_{xx} & 0 & 0 \\ 0 & (1-\alpha)A_{yy} + \alpha A_{zz} & 0 \\ 0 & 0 & (1-\alpha)A_{zz} + \alpha A_{yy} \end{pmatrix} \quad (49)$$

Now $\bar{\mathbf{A}}$ is averaged in the same manner with $\theta = 90°$ and $\phi = 90°$ to account for motion about the y-axis. The motionally averaged tensor, $\bar{\bar{\mathbf{A}}}$, is diagonal with elements

$$\bar{\bar{A}}_{xx} = (1-\alpha)A_{xx} + \alpha^2 A_{yy} + \alpha(1-\alpha)A_{zz}$$
$$\bar{\bar{A}}_{yy} = (1-\alpha)A_{yy} + \alpha A_{zz}$$
$$\bar{\bar{A}}_{zz} = (1-\alpha)^2 A_{zz} + \alpha A_{xx} + \alpha(1-\alpha)A_{yy} \quad (50)$$

The equivalent expression for considering the two motions in the opposite order can be obtained by switching the x- and y-indices in eqs 50. Averaging these two sets of results gives

$$\langle \bar{\bar{A}}_{xx} \rangle = A_{\text{perp}} + {}^1/_2(2\alpha - \alpha^2)(A_{zz} - A_{\text{perp}}) + (1 - \alpha - \alpha^2/2)A^*$$
$$\langle \bar{\bar{A}}_{yy} \rangle = A_{\text{perp}} + {}^1/_2(2\alpha - \alpha^2)(A_{zz} - A_{\text{perp}}) - (1 - \alpha - \alpha^2/2)A^*$$
$$\langle \bar{\bar{A}}_{zz} \rangle = A_{zz} - (2\alpha - \alpha^2)(A_{zz} - A_{\text{perp}}) \quad (51)$$

Numerical calculations show that up to $\alpha = 0.0550$, which corresponds to the highest amplitude of internal motion used in this work, eqs 50 and 51 give nearly identical results. The x- and y-elements of $\bar{\bar{\mathbf{A}}}$ are equal to those of $\langle \bar{\bar{\mathbf{A}}} \rangle$ to within 0.05 G; $\bar{\bar{A}}_{zz}$ is equal to those of $\langle \bar{\bar{A}}_{zz} \rangle$ to within 0.01 G. The variation between the elements of $\bar{\bar{\mathbf{g}}}$ and $\langle \bar{\bar{\mathbf{g}}} \rangle$ is 1×10^{-5}. This demonstrates that the order in which the independent motions about the x- and y-axes are considered does effect the results, but only slightly.

Unification of Averaging Models. It is desirable to put the equations for the elements of $\langle \bar{\bar{\mathbf{A}}} \rangle$ into a form comparable to those of eqs 48. This can be accomplished by making the approximation

$$\langle \bar{\bar{\mathbf{A}}}^* \rangle = {}^1/_2(\langle \bar{\bar{A}}_{xx} \rangle - \langle \bar{\bar{A}}_{yy} \rangle) \approx A^* = {}^1/_2(A_{xx} - A_{yy}) \quad (52)$$

and by neglecting the terms proportional to α^2 (which is valid for small α). With these approximations:

$$\langle \bar{\bar{A}}_{xx} \rangle = A_{\text{perp}} + \alpha(A_{zz} - A_{\text{perp}}) + A^*$$
$$\langle \bar{\bar{A}}_{yy} \rangle = A_{\text{perp}} + \alpha(A_{zz} - A_{\text{perp}}) - A^*$$
$$\langle \bar{\bar{A}}_{zz} \rangle = A_{zz} - 2\alpha(A_{zz} - A_{\text{perp}}) \quad (53)$$

A numerical comparison shows that, up to $\alpha = 0.055$, the exact results in eqs 51 and the approximate expressions in eqs 53 differ by 0.10 G or less for the motionally average A-tensor elements and 1×10^{-5} or less for the motionally averaged g-tensor elements. Equations 51, derived for motion about two orthogonal axes, are equivalent to eqs 48, for motion about a single axis, except for the replacement of α by 2α. This factor of 2 is a direct consequence of going from one motional process to two equivalent motional processes. For multiple independent motional processes, the total mean-squared amplitude of motion is the sum of the mean-squared amplitudes of the individual motions. Thus for independent rotations about two orthogonal axes (x and y):

$$\langle \phi'^2 \rangle_{\text{total}} = \langle \phi'^2 \rangle_x + \langle \phi'^2 \rangle_y \quad (54)$$

If it is assumed that $\langle \phi'^2 \rangle_x = \langle \phi'^2 \rangle_y$ and that, from eq 41, α is approximately equal to the mean-squared amplitude of rotation about either axis, then

$$\langle \phi'^2 \rangle_{\text{total}} = \langle \phi'^2 \rangle_x + \langle \phi'^2 \rangle_y \approx 2\alpha \quad (55)$$

On the other hand, for rotation about a single axis

$$\langle \phi'^2 \rangle_{\text{total}} = \langle \phi'^2 \rangle \approx \alpha \quad (56)$$

Thus, for either one or two-dimensional motion, the motionally averaged hyperfine tensor elements can be written as follows:

$$\langle \bar{\bar{A}}_{xx} \rangle = A_{\text{perp}} + {}^1/_2\langle \phi'^2 \rangle_{\text{total}}(A_{zz} - A_{\text{perp}}) + A^*$$
$$\langle \bar{\bar{A}}_{yy} \rangle = A_{\text{perp}} + {}^1/_2\langle \phi'^2 \rangle_{\text{total}}(A_{zz} - A_{\text{perp}}) - A^*$$
$$\langle \bar{\bar{A}}_{zz} \rangle = A_{zz} - \langle \phi'^2 \rangle_{\text{total}}(A_{zz} - A_{\text{perp}}) \quad (57)$$

The averaged tensor values given in eqs 57 have been used to generate the simulations. These equations are reasonable approximations to the results for both the one axis and two axes of rotation models.

REFERENCES

Allison, S. A. (1986) *Macromolecules 19*, 118–124.
Allison, S. A., & Schurr, J. M. (1979) *Chem. Phys. 41*, 35–59.
Allison, S. A., Shibata, J. H., Wilcoxon, J., & Schurr, J. M. (1982) *Biopolymers 21*, 729–762.
Allison, S., Austin, R., & Hogan, M. (1989) *J. Chem. Phys. 90*, 3843–3854.
Balasubramanian, K., & Dalton, L. R. (1979) *J. Magn. Reson. 33*, 245–260.
Barber, E. J. (1966) *Natl. Cancer Inst. Monogr. 21*, 219–239.
Barkley, M. D., & Zimm, B. H. (1979) *J. Chem. Phys. 70*, 2991–3007.
Beth, A. H., & Robinson, B. H. (1989) in *Biological Magnetic Resonance* (Berliner, L. J., Ed.) Vol. 8, Academic Press, New York.
Bobst, A. M., Kao, S.-C., Toppin, R. C., Ireland, J. C., & Thomas, I. E. (1984) *J. Mol. Biol. 173*, 63–74.
Bobst, A. M., Pauly, G. T., Keyes, R. S., & Bobst, E. V. (1988) *FEBS Lett. 228*, 33–36.
Brandes, R., Vold, R. R., Vold, R. L., & Kearns, D. R. (1986) *Biochemistry 25*, 7744–7751.
Dalton, L. R., Robinson, B. H., Dalton, L. A., & Coffey, P. (1976) in *Advances in Magnetic Resonance* (Waugh, J. S., Ed.) Vol. 8, Academic Press, New York.
Edwards, A. L. (1969) *Statistical Analysis*, 3rd ed., p 68, Holt Rinehart and Winston, New York.
Eimer, W., Williamson, J. R., Boxer, S. G., & Pecora, R. (1990) *Biochemistry 29*, 799–811.
Freed, J. H. (1976) in *Spin Labeling: Theory and Applications* (Berliner, L. J., Ed.) Vol. 1, Academic Press, New York.
Fujimoto, B. S., & Schurr, J. M. (1990) *Nature 344*, 175–178.
Goldstein, H. (1980) *Classical Mechanics*, Addison-Wesley, Reading, MA.
Griffith, O. H., & Jost, P. (1976) in *Spin Labeling: Theory and Applications* (Berliner, L. J., Ed.) Vol. 1, Academic Press, New York.
Hogan, M. E., & Austin, R. H. (1987) *Nature 329*, 263–266.
Hogan, M., Wang, J., Austin, R. H., Monitto, C. L., & Hershkowitz, S. (1982) *Proc. Natl. Acad. Sci. U.S.A. 79*, 3518–3522.
Hogan, M. E., LeGrange, J., & Austin, R. H. (1983) *Nature 304*, 752–754.
Hubbell, W. L., & McConnell, H. M. (1971) *J. Am. Chem. Soc. 93*, 314–326.
Hustedt, E. J. (1989) Ph.D. Thesis, University of Washington, Seattle.
Hwang, J. S., Mason, R. P., Hwang, L.-P., & Freed, J. H. (1975) *J. Phys. Chem. 79*, 489–511.

Johnson, M. E. (1981) *Biochemistry 20*, 3319–3328.
Kao, S.-C., & Bobst, A. M. (1985) *Biochemistry 24*, 5465–5469.
Kearns, D. R. (1984) *CRC Crit. Rev. Biochem. 15*, 237–290.
Kintanar, A., Alam, T. M., Huang, W.-C., Schindele, D. C., Wemmer, D. E., & Drobny, G. (1988) *J. Am. Chem. Soc. 110*, 6367–6372.
Kintanar, A., Huang, W.-C., Schindele, D. C., Wemmer, D. E., & Drobny, G. (1989) *Biochemistry 28*, 282–293.
Kirchner, J. J., Hustedt, E. J., Robinson, B. H., & Hopkins, P. B. (1990) *Tetrahedron Lett. 31*, 593–596.
Lajzerowicz-Bonneteau, J. (1976) in *Spin Labeling: Theory and Applications* (Berliner, L. J., Ed.) Vol. 1, Academic Press, New York.
Levy, G. C., Craik, D. J., Kumar, A., & London, R. E. (1983) *Biopolymers 22*, 2703–2726.
Lipari, G., & Szabo, A. (1980) *Biophys. J. 30*, 489–506.
Lipari, G., & Szabo, A. (1982a) *J. Am. Chem. Soc. 104*, 4546–4559.
Lipari, G., & Szabo, A. (1982b) *J. Am. Chem. Soc. 104*, 4559–4570.
Mailer, C., Danielson, J. D. S., & Robinson, B. H. (1985) *Rev. Sci. Instrum. 56*, 1917–1925.
McConnell, H. M. (1976) in *Spin Labeling: Theory and Applications* (Berliner, L. J., Ed.) Vol. 1, Academic Press, New York.
McConnell, H. M., & McFarland, B. G. (1970) *Q. Rev. Biophys. 3*, 91–136.
Morisett, J. D. (1976) in *Spin Labeling: Theory and Applications* (Berliner, L. J., ed.) Vol. 1, Academic Press, New York.
Nordio, P. L. (1976) in *Spin Labeling: Theory and Applications* (Berliner, L. J., Ed.) Vol. 1, Academic Press, New York.
Pauly, G. T., Thomas, I. E., & Bobst, A. M. (1987) *Biochemistry 26*, 7304–7310.
Pecora, R. (1991) *Science 251*, 893–897.
Robinson, B. H., & Dalton, L. R. (1979) *Chem. Phys. 36*, 207–237.
Robinson, B. H., Forgacs, G., Dalton, L. R., & Frisch, H. L. (1980a) *J. Chem. Phys. 73*, 4688–4692.
Robinson, B. H., Lerman, L. S., Beth, A. H., Frisch, H. L., Dalton, L. R., & Auer, C. (1980b) *J. Mol. Biol. 139*, 19–44.
Robinson, B. H., Thomann, H., Beth, A. H., Fajer, P., & Dalton, L. R. (1985) in *EPR and Advanced EPR Studies of Biological Systems* (Dalton, L. R., Ed.) Chapter 2, CRC Press, Boca Raton.
Robinson, B. H., Slutsky, L. J., & Auteri, F. P. (1992) *J. Chem. Phys. 96*, 2609–2616.
Schultz, S. C., Shields, G. C., & Steitz, T. A. (1991) *Science 253*, 1001–1007.
Schurr, J. M. (1984) *Chem. Phys. 84*, 71–96.
Schurr, J. M., & Schmitz, K. S. (1986) *Annu. Rev. Phys. Chem. 37*, 271–305.
Schurr, J. M., & Fujimoto, B. S. (1988) *Biopolymers 27*, 1543–1569.
Schurr, J. M., Fujimoto, B. S., Wu, P., & Song, L. (1992) in *Topics in Fluorescence Spectroscopy, Volume 3: Biological Applications* (Lakowicz, J. R., Ed.) Plenum Press, New York.
Shibata, J. H., Fujimoto, B. S., & Schurr, J. M. (1985) *Biopolymers 24*, 1909–1930.
Song, L., & Schurr, J. M. (1990) *Biopolymers 30*, 229–237.
Spaltenstein, A., Robinson, B. H., & Hopkins, P. B. (1988) *J. Am. Chem. Soc. 110*, 1299–1301.
Spaltenstein, A., Robinson, B. H., & Hopkins, P. B. (1989a) *Biochemistry 28*, 9484–9495.
Spaltenstein, A., Robinson, B. H., & Hopkins, P. B. (1989b) *J. Am. Chem. Soc. 111*, 2303–2305.
Steinhoff, H.-J., Lieutenant, K., & Schlitter, J. (1989) *Z. Naturforsch. 44c*, 280–288.
Strobel, O. K., Keyes, R. S., & Bobst, A. M. (1990) *Biochemistry 29*, 8522–8528.
Tirado, M. M., & de la Torre, J. G. (1980) *J. Chem. Phys. 73*, 1986–1993.
Van, S. P., Birrel, G. B., & Griffith, O. H. (1974) *J. Magn. Reson. 15*, 444–459.
Wilcoxon, J., & Schurr, J. M. (1983) *Biopolymers 22*, 2273–2321.
Wu, P., Fujimoto, B. S., & Schurr, J. M. (1987) *Biopolymers 26*, 1463–1488.